Jurnal Tribologi 46 (2025) 92-112

MYTRIBOS Malaysian Tribology Society

Jurnal Tribologi

Website : jurnaltribologi.mytribos.org e-issn: 2289-7232

Triboinformatics of texture bump recess variable compliance foil journal bearing

Arokya Agustin S [1], Shravankumar C [1], Arul Jeya kumar A [1], Rao T V V L N [2*]

[1] Department of Mechanical Engineering, SRM Institute of Science and Technology, Kattankulathur, Chengalpattu, INDIA.
[2] MIT INSPIRE, MIT Art, Design and Technology University, Rajbaugh, Loni Kalbhor, Maharashtra-412201, INDIA.
[*]Corresponding author: tvvlnrao@gmail.com

KEYWORDS

Triboinformatics
Foil journal bearing
Machine learning
Wear

ABSTRACT

The data-driven methods using machine learning (ML) algorithms are examined to provide a correlation of the texture bump recess variable compliance foil journal bearing input parameters and the performance characteristics. These estimates are made for higher bearing numbers ($\Lambda \to \infty$) coupled with higher speeds ($\omega \to \infty$) for the texture bump recess variable compliance foil journal bearing. Different top foil texture bump patterns and bump-recess heights are examined. The data points were divided into training and testing sets in the ratio of 80:20. The four different ML models ((i) Random Forest (ii) Decision Trees (iii) Support Vector Machines (SVM) and (iv) Artificial Neural Networks (ANN)) have been used to predict the texture bump recess variable compliance foil journal bearing performance characteristics. The R^2, MAE, and RMSE are used to find the suitability of the predictions. The texture bump recess variable compliance foil journal bearing performance characteristics (α = 1, α_{tb} =2, 10, ε = 0.2, 0.5, 0.8 and respective output values of W, K_{ij} obtained from the analytical model) are explored in relation to the extent (θ_t = 0, 60°, 120°, 180°) and height of the top foil texture bump (H_b = 0.5, 1.5) using triboinformatics.

Received 11 November 2024; received in revised form 2 January 2025; accepted 20 January 2025.
To cite this article: Agustin et al. (2025). Triboinformatics of texture bump recess variable compliance foil journal bearing. Jurnal Tribologi 46, pp.92-112.

NOMENCLATURE

C	Radial clearance, m
h, H	Film thickness, m; $H = h/C$
H_b	Nondimensional height of texture bump
k_{ij}, K_{ij}	Stiffness coefficients, Ns/m; $\bar{K}_{ij} = k_{ij}C/p_aLR$, $K_{ij} = \bar{K}_{ij}/W$, $i,j = x,y$
L	Length of bearing, m
p_a	Ambient pressure, N/m^2
p, P	Pressure, N/m^2; $P = p/p_a$
R	Radius of journal, m
w, W	Static load, N; $W = w/p_aLR$
x, y, X, Y	Coordinates with respect to bearing center, m; $X = x/C$, $Y = y/C$
$\Delta X, \Delta Y$	Displacements (nondimensional) in x and y directions from the equilibrium position
α	Bump foil compliance coefficient
α_{tb}	Texture bump foil compliance coefficient
α_{wa}	Weighted average of bump foil compliance coefficient used in ML models, $\alpha_{wa} = \left(\alpha_{tb}\theta_t + \alpha(2\pi - \theta_t)\right)/2\pi$
ε	Eccentricity ratio
θ	Circumferential coordinate measured from the position fixed to the negative X-axis
θ_t	Angle coordinate measured from position fixed to negative X-axis for texture bump region
φ	Attitude angle
ω	Angular velocity, rad/s
Λ	Bearing number; $\Lambda = 6\mu\omega R^2/p_aC^2$

1.0 INTRODUCTION

The performance characteristics of foil bearings were comprehensively investigated: steady-state characteristics (Heshmat et al., 1983), stiffness and damping coefficients (Peng and Carpino, 1993), optimum radial clearance effects (Radil et al., 2002), geometrical and operational effects (Rubio and San Andres, 2006), and bump foil in double-stage (Kim and San Andres, 2007). The roadmap of challenges and developments in the technology of foil bearings were also highlighted (Samanta et. al., 2019)

The limiting conditions of foil journal bearings at high operating speeds were explored by Peng and Khonsari (2004a and 2004b). The compressible Reynolds equation is simplified at higher bearing number values (higher operating speeds) to calculate the performance of foil journal bearing under the limiting conditions. The researchers have extensively used the Lund's (1987) perturbation method for evaluation of the dynamic analysis of bearings. Based on Peng and Khonsari's limiting conditions analysis, Sawicki and Rao (2005) derived the dynamic coefficients of foil journal bearing.

Agustin et al. (2020) analyzed texturing effects on top foil, derived the limiting pressure gradient solution and determined the coefficients of stiffness on foil journal bearing with using the Lund's (1987) perturbation method. It was determined how much of an effect the top foil

texture bump had, as well as how high it was, on the coefficients of stiffness of a journal foil bearing.

The various stages of research methods in tribology are empirical techniques, experimental methods, theoretical models, and computational simulations. Artificial intelligence and machine learning methods have gained notable attention in tribology. "Tribo-informatics is a multidisciplinary field that combines tribology, data science and numerical simulation tools to study and optimise tribology relevant mechanical systems". Also, this tribo-informatics provides a practical alternative to analytical/numerical/simulation modelling, enabling rapid and accurate predictions of bearing performance under complex operating conditions. The AI & ML methods provide opportunities to explore complex processes in tribological systems. The extended use of AI & ML methods in tribology was emphasized in the areas of the surface topography characterization and the lubricated system design (Rosenkranz et al. 2021). The triboinformatics classify or quantify or optimize the tribological behavior in an efficient or even real-time way (Tremmel and Marian 2022). The AI & ML implementation in tribology has potential to enable development of rapid design optimization tools with significantly reduced computational time (Cartwright et al. 2024). The implementation of triboinformatics in various industries was shown through practical case studies (Zhang and Yin 2024). Ultimately, AI & ML implementation in tribology aspires to enhance the efficiency of problem-solving in tribology (Yin et al. 2024).

Rahman et al., (2023) presented a comprehensive overview of ML algorithms from a tribological perspective. The possibilities of futuristic lubricant design by ML techniques were projected. Marian and Tremmel (2023) presented an overview of physics-informed machine learning (PIML). The PIML approaches are an improvement of traditional machine learning approaches that rely solely on data-driven methods. Fundamental physics is incorporated into machine learning models in PIML approach for optimizing friction, wear, and lubrication phenomena. Yin et al., (2023) reviewed the triboinformatics applications. Yin et al., (2024) presented an outline to elucidate and to inspire the future directions of AI in tribology. A comprehensive overview on the application of ML & AI in basics of tribology, biotribology, green tribology, and related fields was presented (Yin et al. 2024).

Machine learning (ML) algorithms are widely used on many occasions in tribology research. Table 1 provides an overview of recent investigations in triboinformatics. Triboinformatics is used for parametric evaluation of the texture bump recess variable compliance foil journal bearing. The purpose of this study is to investigate limiting stiffness coefficients of texture bump variable compliance foil journal bearing. A limiting pressure and pressure gradient solution for a texture bump variable compliance foil bearing is presented. In the context of texture bump recess variable compliance foil journal bearing, tribo-informatics is used to investigate its performance. Four data sets are generated using numerical simulations across a range of input parameters (these input parameters depend on the bump geometry and compliance, bearing load, eccentricity ratio and stiffness coefficients). Non-dimensional Load bearing capacity (W) is the output parameter for one data set, whereas for the remaining three datasets Eccentricity ratio (ε) is the output parameter. These four datasets are subsequently used to train and develop four different Machine Learning models, i.e., Decision Tree (DT), Random Forest (RF), Support Vector Machines (SVM) and Artificial Neural Networks (ANN). Testing and evaluation metrics highlight the robustness of the developed ML models in predicting the operating parameters (i.e, W and ε) of the texture bump recess variable compliance foil journal bearing, under the influence of four different sets of input parameters. Furthermore, the ML based triboinformatics is a practical alternative to analytical/numerical/simulation modeling.

Table 1: Triboinformatics models.

Tribological investigations	ML models	Reference
Input		
Wear and friction of aluminum (Al) base alloys	KNN, SVM, ANN, RF, GBM	Hasan et al., (2021)
Wear and friction of Al-graphene metal matrix composites	KNN, SVM, ANN, RF, GBM	Hasan et al., (2022a)
Wear and friction of aluminum-graphite composites	KNN, SVM, ANN, RF, GBM	Hasan et al., (2022b)
Wear of AZ91 alloy under sliding conditions	ANN, SVR, RF	Aydin and Durgut (2021)
Friction coefficient in journal bearings	ANN, SVM, RT	Baş and Karabacak (2023)
ZA-27 alloys with manganese (Mn) additions	DT, RF, ADABoost, GBoost, XGBoost	Hulipalled et al., (2023)
EHL simulations	SVM, GPR, ANN	Marian et al., (2023)
Tribology of UHMWPE/SiC polymer composites	SVMs, DTs, RFs, KNNs, ANNs	Mohammed et al., (2023)
Friction and wear of experiments, and condition monitoring	SVM, PR, ANN, NB, DT	Rahman et al., (2023)
Tribology of copper/aluminum-graphite composites	SVM, KNN, RF, XGBoost, LSBoost	Ning et al. (2024)
Wear depth prediction	RF, KNN, XGB, SVM	Zhu et al., (2024)
Tribo-informatics case studies	ANN, SVM, KNN, RF	Zhang and Yin (2024)

Triboinformatics (in combination with machine learning models) can provide many novel insights about journal bearing design as follows:

(i) Analyze datasets to identify which input parameters (e.g., bump geometry, compliance, load, stiffness coefficients) most significantly influence key performance parameters like nondimensional load capacity (W) and eccentricity ratio (ε).
(ii) Predict the bearing performance parameters (W and ε) for different sets of operating conditions (e.g, different loads, bump geometry, compliance etc.)
(iii) Capture the nonlinear behaviour of the journal bearing, arising due to complex interactions between geometry, compliance and operating loads.
(iv) Evaluate large number of texture configurations to recommend optimal designs that maximize load capacity and minimize friction/wear

The primary objectives of this study focusing on journal bearings (specifically, texture bump recess variable compliance foil journal bearing) are stated as follows:

(i) Mathematical modelling and Numerical analysis: Development and analysis of mathematical models to determine the limiting values of non-dimensional load capacity (W) and stiffness coefficients (K_{ij}) for the journal bearing under study.
(ii) Development of Tribo-informatics Models: Leverage Machine Learning Algorithms to create and evaluate tribo-informatics models as a practical and efficient alternative, for

prediction of key performance metrics, such as non-dimensional load capacity (W) and eccentricity ratio (ε) across different sets of input parameter configurations.

2.0 SYSTEM MODELLING

The necessary conditions for very high-speed operation of foil journal bearing ($\Lambda \rightarrow \infty$) obtained by simplifying the compressible Reynolds equation is (Peng and Khonsari, 2004)

$$\frac{\partial(PH)}{\partial\theta} = 0 \tag{1}$$

The schematic of texture bump foil is shown in Figure 1. The texture bump region (Fig. 1a) extends along circumferential direction from the position fixed to negative X-axis (load line depicted in Fig. 1b). The texture bump region is considered on the top foil surface. The texture bump foil bearing nondimensional film thickness is:

$$H = 1 + \varepsilon\, cos(\theta - \varphi) - H_b + \alpha(P - 1) \tag{2}$$

The steady state pressure and pressure gradients are obtained by infinitesimal perturbation of the simplified compressible Reynolds equation. The pressure distribution and film thickness for infinitesimally small perturbations about the journal steady state is:

$$P = P_o + P_x \Delta X + P_y \Delta Y \tag{3}$$

$$H = H_o + H_x \Delta X + H_y \Delta Y \tag{4}$$

where

$$H_o = 1 + \varepsilon_o\, cos(\theta - \varphi_o) - H_b + \alpha(P_o - 1), \quad H_x = cos\,\theta + \alpha P_x, \qquad H_y = sin\,\theta + \alpha P_y \tag{5}$$

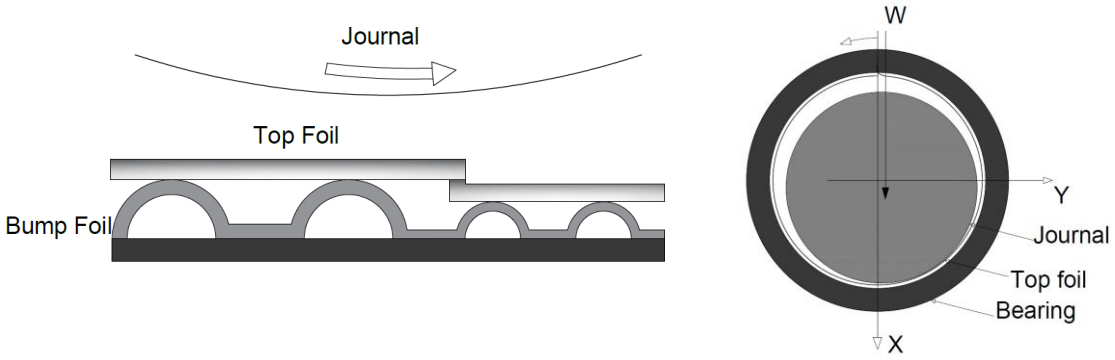

1a: texture bump foil 1b: foil journal bearing

Figure 1: Schematic of texture bump recess variable compliant foil journal bearing

Substituting Eqs. (3-4) in Eq. (1), the steady state and dynamic simplified compressible Reynolds equations are

$$\frac{\partial(P_o H_o)}{\partial\theta} = 0 \tag{6}$$

$$\frac{\partial}{\partial\theta}(P_o H_x + P_x H_o) = 0 \tag{7}$$

$$\frac{\partial}{\partial\theta}\left(P_o H_y + P_y H_o\right) = 0 \tag{8}$$

The texture bump foil bearing limiting pressure distribution is obtained by solving Eq. (6) using the pressure boundary conditions at inlet ($\theta = 0$) as (Peng and Khonsari, 2004)

$$P_o = \frac{1+\varepsilon_o \cos\varphi_o - H_b}{1+\varepsilon_o \cos(\theta-\varphi_o) - H_b + \alpha(P_o-1)} \quad (9)$$

The limiting pressure is simplified from Eq. (9) as

$$P_o = \frac{-(1+\varepsilon_o \cos(\theta-\varphi_o) - H_b - \alpha) + \sqrt{(1+\varepsilon_o \cos(\theta-\varphi_o) - H_b - \alpha)^2 + 4\alpha(1+\varepsilon_o \cos\varphi_o - H_b)}}{2\alpha} \quad (10)$$

Substituting Eq. (5) in Eqs. (7-8), reduce to

$$\frac{\partial}{\partial\theta}\left(P_o \cos\theta + P_x(\alpha P_o + H_o)\right) = 0 \quad (11)$$

$$\frac{\partial}{\partial\theta}\left(P_o \sin\theta + P_y(\alpha P_o + H_o)\right) = 0 \quad (12)$$

The boundary conditions are:

$$P_o = 1; P_x = P_y = 0 \text{ at } \theta = 0 \quad (13)$$

$$P_x = \frac{1-P_o \cos\theta}{1-\alpha+2\alpha P_o+\varepsilon_o \cos(\theta-\varphi_o)-H_b} \quad (14)$$

$$P_y = \frac{-P_o \sin\theta}{1-\alpha+2\alpha P_o+\varepsilon_o \cos(\theta-\varphi_o)-H_b} \quad (15)$$

The nondimensional pressure is integrated to obtain the limiting nondimensional load as

$$\begin{Bmatrix} F_x = W \\ F_y = 0 \end{Bmatrix} = \int_{\theta=0}^{\theta=2\pi} P_o \begin{Bmatrix} \cos\theta \\ \sin\theta \end{Bmatrix} d\theta \quad (16)$$

The bearing stiffness coefficients $K_{xx}, K_{yx}, K_{xy}, K_{yy}$ are evaluated from pressure perturbations as

$$\begin{Bmatrix} K_{xj} \\ K_{yj} \end{Bmatrix} = \int_{\theta=0}^{\theta=2\pi} P_j \begin{Bmatrix} \cos\theta \\ \sin\theta \end{Bmatrix} d\theta \qquad \text{for} \qquad j = x, y \quad (17)$$

3.0 ML METHODOLOGY

The specific input & output parameters for texture bump recess variable compliance foil journal bearings considered in this study are as follows: angle coordinate measured from position fixed to negative X-axis for texture bump region (θ_t); nondimensional height of texture bump (H_b); weighted average of bump foil compliance coefficient used in ML models (α_{wa}); nondimensional stiffness coefficients of journal bearing (K_{ij}); nondimensional load capacity (W); eccentricity ratio (ε).

The four ML regression-based methods developed for prediction of output features, Load and Eccentricity are: ANN, SVM, Random Forest and Decision Trees. The different steps are as follows: (i) data collection and processing (ii) input and output features (iii) Machine Learning model (iv) optimisation of model hyper-parameters (v) training, testing and evaluation of the performance of the ML model.

Following are the evaluation metrics for Regression Tasks: R^2: Variance in the data explained by the model, Mean Absolute Error (MAE): Average absolute difference between predictions and actual values; Root Mean Squared Error (RMSE): Average of the squared differences between predictions and actual values.

R^2 explains how much of the variance in the target variable is explained by the model. R^2=1 explains perfect fit; R^2=0 model explains no variance, predictions are as good as the mean; R^2<0 model performs worse than a constant mean prediction.

$$R^2 = 1 - \frac{\sum_{i=1}^{n}(y_i - \hat{y}_i)^2}{\sum_{i=1}^{n}(y_i - \bar{y})^2} \quad (18)$$

Here, y_i is the actual value, $\hat{y}_i$ is the predicted value, $\bar{y}$ is the mean and n is the number of observations. By explaining the variance, the model demonstrates its ability to uncover the underlying patterns or relationships in the data.

MAE (Mean Absolute Error) represents the average magnitude of errors between predicted and actual values, ignoring their positive or negative direction.

$$MAE = \frac{1}{n}\sum_{i=1}^{n} |y_i - \hat{y}_i| \tag{19}$$

MAE gives an intuitive measure of the prediction accuracy for W and ε.

RMSE (Root Mean Square Error) measures the square root of the average squared differences between predicted and actual values, penalizing large errors more than MAE.

$$RMSE = \sqrt{\frac{1}{n}\sum_{i=1}^{n}(y_i - \hat{y}_i)^2} \tag{20}$$

It highlights the presence of large deviations in predictions, which may be critical for applications where large errors in W and ε significantly impacts journal bearing performance.

The datasets have been generated so as to predict (a) nondimensional load (W) and (b) eccentricity ratio (ε), for different sets of input features. The different sets of input features highlight the robustness of the machine learning model predictions under different sets of operating conditions. The bump foil compliance coefficient, α, is modified and taken as the weighted average of the bump foil compliance coefficient to be used in the machine learning models: $\alpha_{wa} = \left(\alpha_{tb}\theta_t + \alpha(2\pi - \theta_t)\right)/2\pi$.

Data processing is important for better prediction using ML algorithm. Some of the common needs for data pre-processing include missing data, outlier data, different range of features: normalizing or scaling, reducing data volume using PCA. The outliers are removed from the datasets, by using their Z-scores, which measures how far a data point deviates from its meaning in terms of its standard deviation. In this work, data points with Z-scores that exceed a threshold value of 3 (common usage) are considered as outliers and are eliminated from the data set.

The Z-score is given using the formula: z_scores = abs((X − mean(X)) ./ std(X)). Z-score of the datasets is used for detecting outliers as well as for preprocessing the datasets for feature standardization, for e.g., features like journal bearing stiffness and compliance are standardized to avoid dominance by features with larger ranges.

The analysis of four different ML models ((i) Random Forest (ii) Decision Trees (iii) Support Vector Machines (SVM) and (iv) Artificial Neural Networks (ANN)) to solve the regression problem and estimate the output features are presented.

The selection criteria for Machine Learning models include:

(a) The models should be efficient in capturing the nonlinear patterns in data. This is required because the non-dimensional load capacity (W) and the eccentricity ratio (ε) are influenced by complex, non-linear interactions between the input parameters (i.e., bump geometry, compliance, load and stiffness coefficients)

(b) The models should be highly suitable for a range of dataset sizes. SVM is efficient for small to medium datasets; ANN performs well for medium datasets, especially with the aid of hyper-parameter tuning and preprocessing; Random Forest and decision trees perform well across a range of dataset sizes.

Every ML model has its own distinct list of hyper-parameters, whose values are crucial for the efficient prediction of the target features. Table 2 gives as summary of different ML models and their key hyper-parameters used in the process of feature prediction.

Table 2: ML model parameters for estimation of load and eccentricity.

ML model	Regression function	Hyper Parameters (MATLAB)
Random Forest	fitrseensemble()	NumLearningCylces = 100, MaxNumSplits = 10, MaxFeatures = 5 (W and WEC datasets) Max Features = 8 (STEC dataset) MaxFeatures = 9 (WSTEC dataset)
Decision Trees	fitrtree()	MaxDepth = 3, MaxNumSplits = 5 (W, STEC and WSTEC dataset) MaxDepth = 4, MaxNumSplits = 5 (WEC dataset) MinLeafSize = 1 (default for all)
SVM	Predict()	C_Value = 100 (W and WEC), C_Value = 0.1 (STEC and WSTEC) Epsilon = 0.01 (W and WEC), Epsilon = 0.1 (STEC and WSTEC) Kernel Function = RBF (W and WEC), Kernel Function = Linear (STEC and WSTEC)
ANN	trainlm()	Hidden Layer Size: 5, Learning Rate: 0.0500 and Number of Epochs: 1000 (WSTEC and W) Hidden Layer Size: 5, Learning Rate: 0.1 and Number of Epochs: 1500 (WEC) Hidden Layer Size: 5, Learning Rate: 0.0500 and Number of Epochs: 1500 (STEC)

Random Forest

In Random Forest NumLearningCycles is equivalent to n_estimators in python, i.e. the number of decision trees in the ensemble; MaxNumSplits is equivalent to max_depth in python, i.e., number of splits each individual tree in the ensemble can make. These are default to 100 and 10. max_features correspond to the total number of available features in each dataset.

Support Vector Machines

For SVM, the following hyper parameters were considered. C Value: It stands for regularisation parameter. In regression, the regularization parameter controls the complexity of the model and helps prevent overfitting by adding a penalty term to the loss function. This penalty discourages the model from fitting too closely to the training data, which can improve its generalization to new, unseen data. Different types of regression models use various regularization techniques and parameters, such as Lasso, Ridge, and Elastic Net. Higher C values penalize errors more, causing the model to fit the training data more closely. This can reduce bias but increase variance, leading to potential overfitting. Lower C values allow more tolerance for errors, resulting in a softer margin that may improve generalization but can lead to underfitting if too low.

Epsilon values: Epsilon defines a margin of tolerance around the regression line within which errors are ignored. In other words, it specifies an epsilon-insensitive zone around the predicted values, where the model does not penalize errors. This means that if the predicted value falls within ±epsilon of the actual value, there's no penalty for the error.

Small Epsilon values: The model tries to fit the data points more tightly, potentially leading to higher sensitivity to noise and overfitting.

Large Epsilon values: A wider margin is tolerated, which can lead to a smoother model that may underfit but generalizes better.

Kernel function: the kernel function is a fundamental component that transforms the data into a higher-dimensional space to make it easier to fit a linear regression line. By mapping the data to a higher-dimensional space, SVM can capture non-linear relationships in the data without explicitly calculating coordinates in that space. Common kernel functions inlcude: Linear, Poylnomial, RBF and Sigmoid.

In this work, hyper parameters for the SVM model were optimised using Grid Search method. The grid search parameters chosen were as follows.

C – regularisation parameter – 0.1, 1, 10, 100

Epsilon – Tolerance margin – 0.01, 0.1, 0.5, 1

Kernel function – Linear, RBF, Polynomial

The best hyper parameters obtained for each dataset are tabulated as follows (Table 3):

Table 3: ML model parameters for estimation of load and eccentricity.

Parameter	**W**	**ε_WEC**	**ε_STEC**	**ε_WSTEC**
C-value [0.1, 1, 10, 100]	100	100	0.1	0.1
Epsilon – value [0.01, 0.1, 0.5, 1]	0.01	0.01	0.1	0.1
Kernel function [Linear, RBF, Polynomial]	RBF	RBF	Linear	Linear

Artificial Neural Network

Artificial Neural Network (ANN) models are optimally built. The process involves the following steps: (i) Data pre-processing (ii) Training and testing data sets (iii) optimal ANN model (iv) feed forward and training the ANN model using gradient descent (v) Evaluation metrics (vi) results visualization.

Building the ANN model: For all the data sets, the data is split into 70% for training and 30% for testing. One hidden layer is chosen to start with. Levenberg-Marquardt Gradient Descent algorithm was used for training. Optimal values are obtained for the hyper-parameters, i.e., number of neurons in the hidden (5, 10, 15), learning rates (0.01, 0.01 and 0.1) and number of epochs (500, 1000, 1500); where the numbers within the brackets represent the hyper-parameter ranges among which the optimal values are obtained using grid search. It defines a range of possible values for each hyper-parameters and then evaluates the model performance for each possible combination (27 possible combinations in the present case) of these hyper-parameters. Optimized hyper-parameter for the ANN models are presented in Table 4 and 5.

Table 4: Best HyperParameters obtained for ANN model using Grid Search method

Parameter	**W**	**ε_WEC**	**ε_STEC**	**ε_WSTEC**
Best Hidden Layer Size	5	5	5	5
Best Learning Rate	0.05	0.1	0.05	0.05
Best Number of Epochs	1000	1500	1500	1000

Table 5: Details of ANN parameters used for prediction of load and eccentricity.

Parameter	**W**	**ε_WEC**	**ε_STEC**	**ε_WSTEC**
No. of hidden layers	1	1	1	1
No. of Neurons per layer (Input/ Hidden/ Output)	4/20/1	4/20/1	7/20/1	8/20/1
Learning rate	0.05	0.1	0.05	0.05
Validation checks (stopped/target)	5 / 6 Best val. is 0.056931 (MSE) at epoch 1	6/ 6 Best val. is 0.025904 (MSE) at epoch 0	6/ 6 Best val. is 0.019502 (MSE) at epoch 5	4/ 6 Best val. is 0.0849 (MSE) at epoch 2
Activation function	Sigmoid (for Hidden layer) Ramp (for output layer)			
No. of Epochs (stopped value)	6	7	11	6
Gradient value at the final epoch	1.31×10^{-13} Mu = 1×10^{-9}	0.00171 Mu = 0.0001	0.000139 Mu = 1e-9	9.55×10^{-8} Mu = 1×10^{-9}

Decision Tree

Some of the hyper parameters of the decision tree are as follows. MaxDepth is the longest path from the root node to any leaf node, MinLeafSize is the Minimum number of samples required for a node to be a leaf and MaxNumSplits is the Total number of splits (internal nodes) in the tree. Decision Tree for datasets is presented in Figures 2-4.

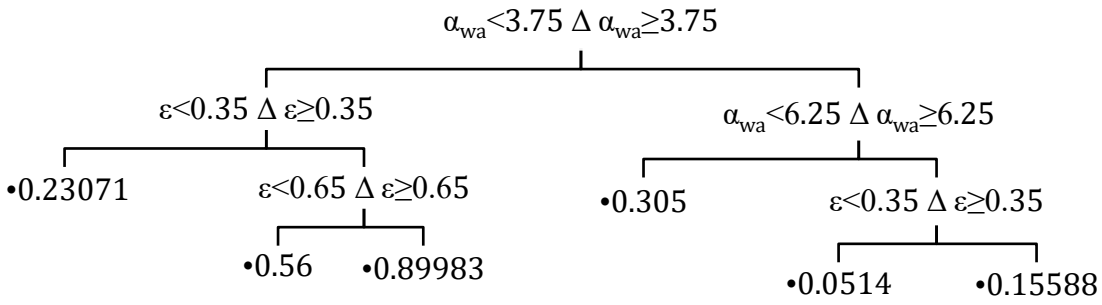

Figure 2: Decision Tree for W dataset

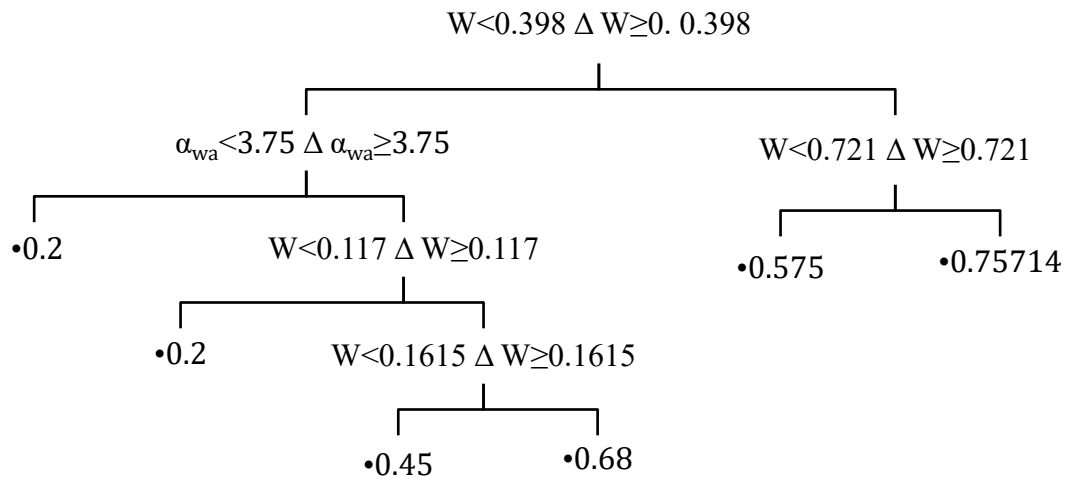

Figure 3: Decision Tree for WEC dataset

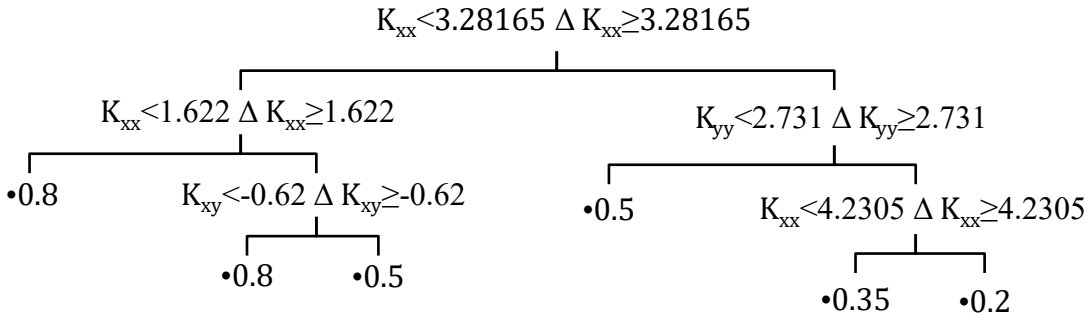

Figure 4: Decision Tree for STEC and WSTEC datasets

4.0 RESULTS AND DISCUSSION

The limiting values of load capacity for a texture bump foil bearing are presented. Results of nondimensional load capacity (W) and nondimensional stiffness coefficients (K_{ij}) are presented for the following parameters: nondimensional height of texture bump (H_b = 0.5, 1.5); bump foil compliance coefficient (α = 1); texture bump foil compliance coefficient (α_{tb} = 2, 10); eccentricity ratio (ε = 0.2, 0.5, 0.8); angle coordinate measured from position fixed to negative X-axis for texture bump region (θ_t = 0, 60°, 120°, 180°). The previous works (Agustin et al., 2020 & Sawicki and Rao, 2005) presented the modeling of limiting nondimensional stiffness coefficients of plain & textured fixed compliance foil journal bearing. This work highlights the impression of triboinformatic methods for texture bump recess variable compliance foil journal bearing using machine learning (ML) algorithms.

Figure 5 shows the nondimensional load capacity of a texture bump variable compliance foil journal bearing. The nondimensional load capacity (W) increases with increasing nondimensional texture bump height (H_b) for a critical value of texture bump extent (θ_t). The nondimensional load capacity (W) does not vary with increasing nondimensional texture bump height (H_b) for all the bump foil compliance coefficients (α_{tb}=1, α=2 and α_{tb}=1, α=10) until a critical value of texture bump extent (θ_t). The nondimensional load capacity (W) increases once a critical value of texture bump extent (θ_t) is reached, i.e., around 120^0 as shown in Fig. 5.

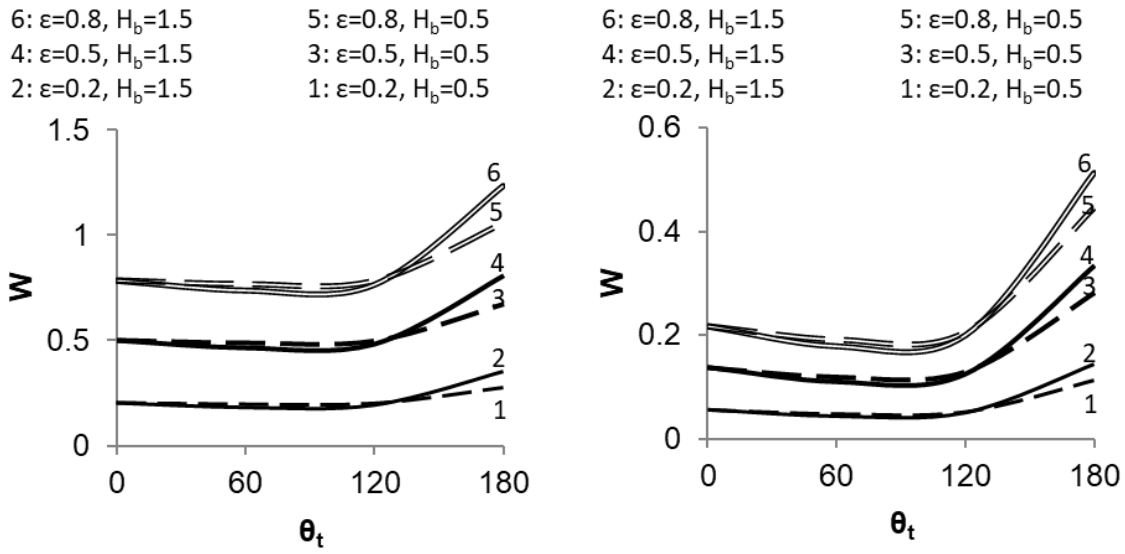

5a: W (α_{tb}=1, α=2) 5b: W (α_{tb}=1, α=10)

Figure 5: Nondimensional load capacity.

The limiting values of nondimensional stiffness coefficients (K_{ij}) for texture bump foil bearing are presented in Figs. 6a-6d. The nondimensional stiffness coefficients (K_{ij}) vary with the extent of texture bump region (θ_t) and nondimensional texture bump height (H_b) as shown in Figs. 6a-6d. The nondimensional stiffness coefficients (K_{ij}) showed higher variation with increasing nondimensional texture bump height (H_b) at lower eccentricity ratio (ε=0.2). The nondimensional stiffness coefficients perpendicular to load line (K_{yj}) showed variation with increasing extent of texture bump region (θ_t). The nondimensional pressure gradients with perturbation along the direction perpendicular to load line (P_y) are significantly influenced by the extent of texture bump region (θ_t) from position fixed to negative X-axis. Similar to the nondimensional load capacity (W), as bump foil compliance coefficient increases from α=2 to α=10, the nondimensional stiffness coefficients (K_{ij}) do not show considerable variation with increasing nondimensional texture bump height (H_b=0-1.5).

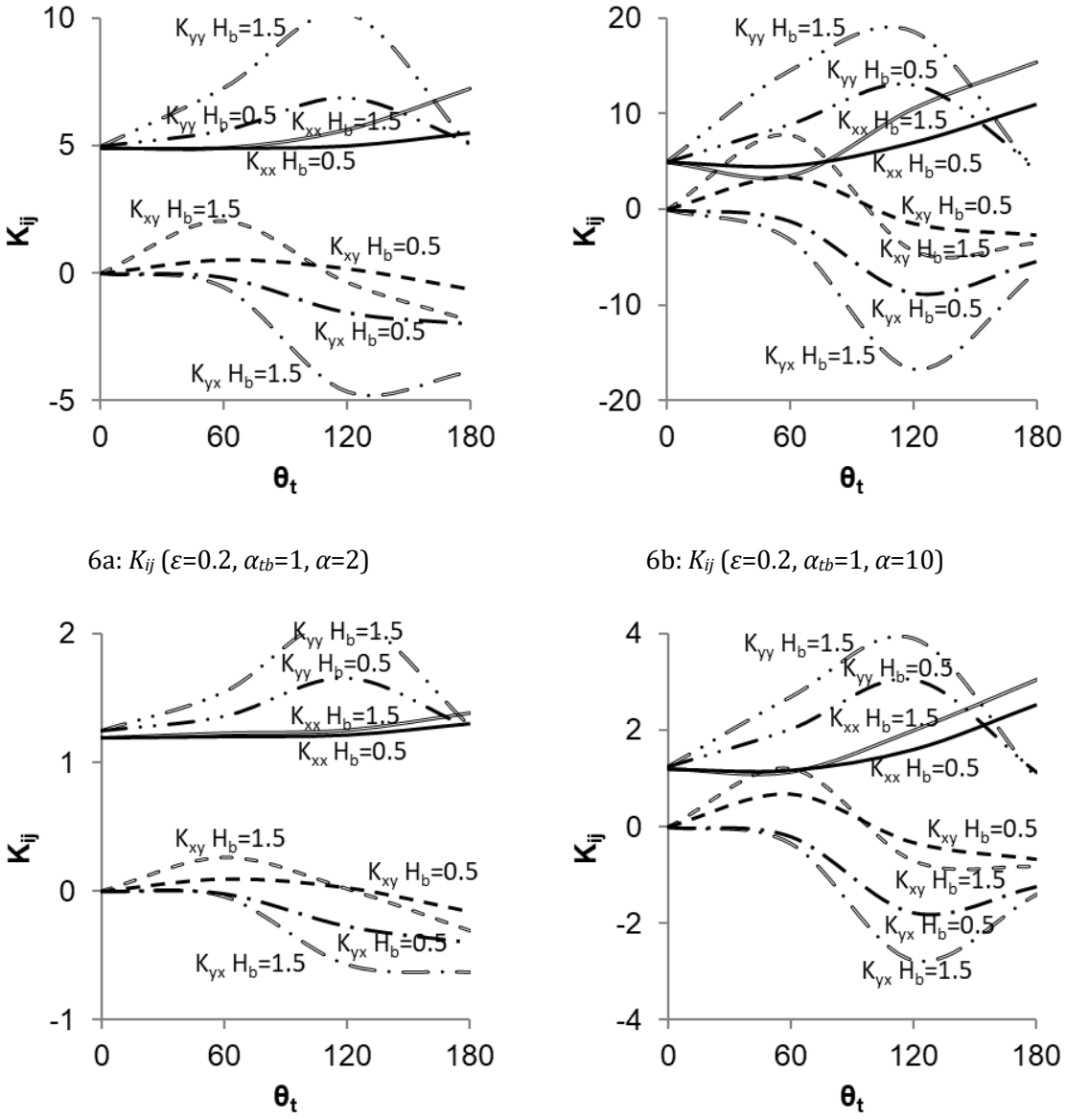

6a: K_{ij} (ε=0.2, α_{tb}=1, α=2)

6b: K_{ij} (ε=0.2, α_{tb}=1, α=10)

6c: K_{ij} (ε=0.8, α_{tb}=1, α=2).

6d: K_{ij} (ε=0.8, α_{tb}=1, α=2).

Figure 6: Nondimensional stiffness coefficients.

In this work, four datasets are considered for the machine learning prediction purpose. Table 6 shows the Input/Output features for each dataset with 48 data samples.

The holdout method is a fundamental approach to training, testing, and evaluating machine learning models. It is simple and widely used, especially when working with a single dataset. In the holdout method, the original dataset is divided into two parts: training set and test set. 80% of the data is assigned to the training set, although this split can vary based on the dataset size

and other factors. 80:20 ratios imply that 80% of the dataset is allocated for training while 20% of the dataset is retained for testing. The reason for using an 80:20 ratio for splitting the dataset is attributed to the size and nature of the dataset. Allocating 80% of the data to training set ensures that the model has enough data to learn patterns and relationships between input and output features. Whereas, allocating 20% testing data provides reasonable amount of unseen data to evaluate the model's generalization capability. More training data means improved model ability to learn patterns, leading to better performance and reducing the risk of underfitting. Also, sufficient testing samples are allocated to ensure robust evaluation and to reduce the risk of over estimating performance.

Four datasets were used in this work: (i) W, (ii) ε_WEC, (iii) ε_STEC, (iv) ε_WSTEC. Table 6 shows the input/output features for each dataset. The comparison of the Actual vs Predicted values of these four datasets used in this work are depicted in Figure 7: Nondimensional load ((i) W) and Eccentricity ratio ((ii) ε_WEC, (iii) ε_STEC, (iv) ε_WSTEC). The R^2, MAE, RMSE values of these four datasets used in this work ((i) W, (ii) ε_WEC, (iii) ε_STEC, (iv) ε_WSTEC) are tablulated in Tables 7-10 respectively.

Table 6: Input/Output features for each dataset.

Features	***W***	***ε_WEC***	***ε_STEC***	***ε_WSTEC***
Input	θ_t, ε, H_b, α_{wa}	θ_t, W, H_b, α_{wa}	θ_t, H_b, α_{wa}, K_{ij}	θ_t, W, H_b, α_{wa}, K_{ij}
Output	W	ε	ε	ε

Table 7: Nondimensional load capacity (W).

Parameter	**Decision Tree**	**ANN**	**Random Forest**	**SVM**
R^2	0.9126	0.9966	0.995	0.9521
MAE	0.0622	0.0131	0.0137	0.0568
RMSE	0.0766	0.0003	0.0182	0.0617

Table 8: Eccentricity ratio (ε_WEC).

Parameter	**Decision Tree**	**ANN**	**Random Forest**	**SVM**
R^2	0.7585	0.9652	0.9184	0.9743
MAE	0.0912	0.0316	0.0431	0.0338
RMSE	0.1258	0.0457	0.0709	0.0392

Table 9: Eccentricity ratio (ε_STEC).

Parameter	**Decision Tree**	**ANN**	**Random Forest**	**SVM**
R^2	1	0.9821	0.9905	0.8527
MAE	0	0.0188	0.016	0.0814
RMSE	0	0.0328	0.0239	0.0849

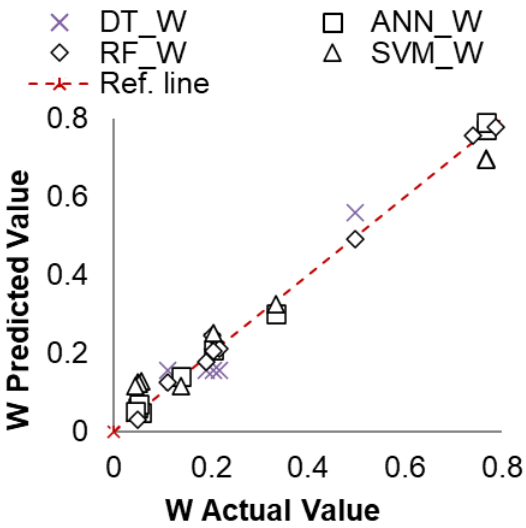

7a: W

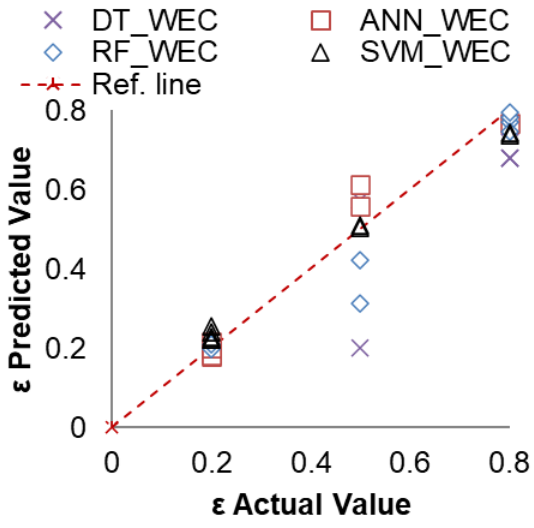

7b: ε_WEC

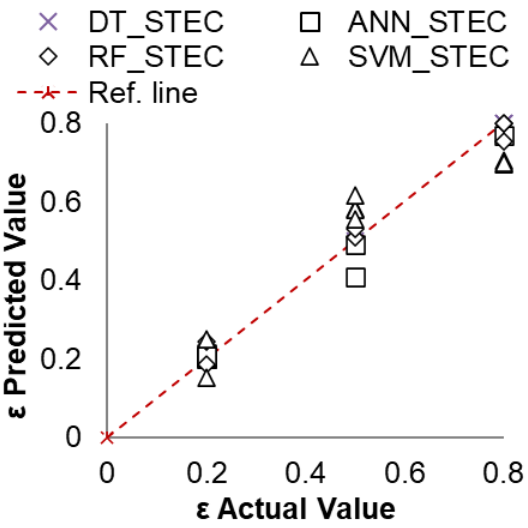

7c: ε_STEC

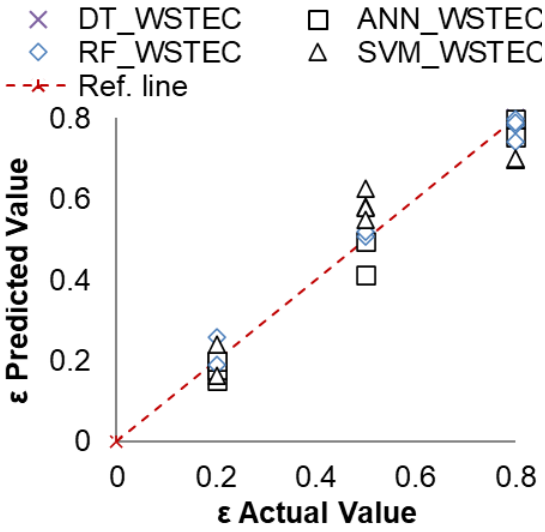

7d: ε_WSTEC

Figure 7: Nondimensional load and Eccentricity ratio (Actual vs Predicted).

Table 10: Eccentricity ratio (ε_WSTEC).

Parameter	Decision Tree	ANN	Random Forest	SVM
R^2	1	0.8938	0.9861	0.8516
MAE	0	0.0463	0.0199	0.0798
RMSE	0	0.0781	0.0289	0.0852

Highest predictive accuracy is indicated by the MAE being close to zero. The key reasons behind its performance include simple and interpretable datasets of the present work.

- ANN and Random Forest demonstrate the highest predictive accuracy for prediction of nondimensional load capacity W;
- ANN, SVM and Random Forest demonstrate the highest predictive accuracy for prediction of Eccentricity ratio (ε_WEC);
- Decision tree, Random Forest and ANN demonstrate the highest predictive accuracy for prediction of Eccentricity ratio (ε_STEC);
- Random Forest and ANN demonstrate the highest predictive accuracy for prediction of Eccentricity ratio (ε_WSTEC);

The validation of data is essential to ensure the robustness and reliability of the findings. Cross-validation of machine learning models can enhance data validation. K-fold cross-validation splits the data into multiple folds and iteratively trains and tests the models to ensure consistent performance across all subsets of data. The models' performance metrics (e.g. R^2, MAE, RMSE) are averaged across all folds to provide a more reliable estimate. The K-fold cross-validation is performed for the same hyper-parameters which were used in the earlier results. An R^2 value close to 1 indicates that the model is close to 100% of the variance in the target variable across all folds. The MAE shows how close predictions are to the actual values, on average. The standard deviation (± value) indicates some variability in error across folds, but it is within a reasonable range and maintains overall accuracy. RMSE gives the average magnitude of the error, with a stronger emphasis on larger errors compared to MAE due to squaring the differences. Low values indicate that the predictions are generally close to the actual values. Standard deviation values can show slightly more variability compared to MAE, indicating large errors in some folds, but these instances are not frequent. The K-fold cross-validation of Decision Tree, ANN, Random Forest, SVM is tablulated in Tables 11-14 respectively.

Table 11: Decision Tree: K-fold cross-validation, K = 5 (chosen).

	W			**WEC**		
Fold	**R^2**	**MAE**	**RMSE**	**R^2**	**MAE**	**RMSE**
1	0.82455	0.11036	0.14053	0.73384	0.10952	0.14592
2	0.27915	0.089624	0.11954	0.0016582	0.17975	0.20983
3	0.8846	0.064224	0.073373	0.6782	0.0975	0.12735
4	0.73981	0.12822	0.19109	0.74895	0.08625	0.14181
5	0.91964	0.037822	0.069185	0.477	0.10595	0.14464
Mean Performance Metrics:	0.7296 ± 0.2608	0.0861 ± 0.0360	0.1187 ± 0.0506	0.5279 ± 0.3136	0.1158 ± 0.0369	0.1539 ± 0.0321
	STEC			**WSTEC**		
Fold	**R^2**	**MAE**	**RMSE**	**R^2**	**MAE**	**RMSE**
1	0.875	0.033333	0.1	0.875	0.033333	0.1
2	0.79592	0.03	0.094868	0.38776	0.09	0.16432
3	0.64286	0.06	0.13416	0.64286	0.06	0.13416
4	1	0	0	1	0	0
5	1	0	0	1	0	0
Mean Performance Metrics:	0.8628 ± 0.1505	0.0247 ± 0.0253	0.0658 ± 0.0619	0.7811 ± 0.2639	0.0367 ± 0.0390	0.0797 ± 0.0762

Table 12: ANN: K-fold cross-validation, K = 5 (chosen).

	W (HiddenLayerSize = 5, LearningRate = 0.05, Epochs = 1000)			**WEC** (HiddenLayerSize = 5, LearningRate = 0.1, Epochs = 1500)		
Fold	**R^2**	**MAE**	**RMSE**	**R^2**	**MAE**	**RMSE**
1	0.77674	0.10558	0.13832	0.57449	0.137928	0.159783
2	0.9931	0.014862	0.017966	0.83218	0.074849	0.102088
3	-0.089617	0.12853	0.1568	0.45941	0.100822	0.141236
4	0.35011	0.12018	0.16213	0.51279	0.124147	0.173942
5	0.56665	0.18451	0.22843	-0.10468	0.203630	0.247732
Mean Performance Metrics:	0.5194 ± 0.4161	0.1107 ± 0.0614	0.1407 ± 0.0766	0.4548 ± 0.3439	0.1283 ± 0.0485	0.1650 ± 0.0536
	STEC (HiddenLayerSize = 5, LearningRate = 0.05, Epochs = 1500)			**WSTEC** (HiddenLayerSize = 5, LearningRate = 0.05, Epochs = 1000)		
Fold	**R^2**	**MAE**	**RMSE**	**R^2**	**MAE**	**RMSE**
1	0.98795	0.017154	0.026884	0.93455	0.053626	0.062667
2	0.47748	0.14103	0.18013	0.83773	0.072422	0.10038
3	-0.18108	0.17108	0.20876	0.43824	0.12052	0.14398

4	0.83453	0.049703	0.10137	0.7754	0.082889	0.1181
5	0.80223	0.080186	0.10482	0.72844	0.1064	0.12283
Mean Performance Metrics:	0.5842 ± 0.4664	0.0918 ± 0.0636	0.1244 ± 0.0718	0.7429 ± 0.1870	0.0872 ± 0.0267	0.1096 ± 0.0305

Table 13: Random Forest: K-fold cross-validation, K = 5 (chosen).

	W			**WEC**		
Fold	**R^2**	**MAE**	**RMSE**	**R^2**	**MAE**	**RMSE**
1	0.9441	0.05573	0.079323	0.66132	0.13431	0.1646
2	0.97764	0.015229	0.021053	0.77343	0.069112	0.099958
3	0.9834	0.021885	0.027826	0.94633	0.044254	0.052011
4	0.97627	0.031375	0.057709	0.6662	0.10318	0.16352
5	0.99389	0.014493	0.019071	0.52967	0.081635	0.13716
Mean Performance Metrics:	0.9751 ± 0.0186	0.0277 ± 0.0171	0.0410 ± 0.0265	0.7154 ± 0.1554	0.0865 ± 0.0342	0.1234 ± 0.0478
	STEC			**WSTEC**		
Fold	**R^2**	**MAE**	**RMSE**	**R^2**	**MAE**	**RMSE**
1	0.87479	0.049275	0.10009	0.88281	0.049008	0.096824
2	0.75879	0.058288	0.10314	0.75593	0.054547	0.10375
3	0.83761	0.063002	0.090467	0.75087	0.072968	0.11205
4	0.9566	0.035372	0.058962	0.96846	0.0312	0.050262
5	0.91803	0.037331	0.057259	0.9396	0.030302	0.049152
Mean Performance Metrics:	0.8692 ± 0.0762	0.0487 ± 0.0123	0.0820 ± 0.0223	0.8595 ± 0.1017	0.0476 ± 0.0178	0.0824 ± 0.0303

Table 14: SVM: K-fold cross-validation, K = 5 (chosen).

	W (Kernel Function: rbf, BoxConstraint (C): 100, Epsilon: 0.01)			**WEC** (Kernel Function: rbf, BoxConstraint (C): 100, Epsilon: 0.01)		
Fold	**R^2**	**MAE**	**RMSE**	**R^2**	**MAE**	**RMSE**
1	0.34234	0.17255	0.23739	0.18718	0.19302	0.22084
2	0.85184	0.076732	0.083234	0.83385	0.077574	0.10158
3	0.60382	0.084275	0.094549	0.61225	0.088925	0.11962
4	0.4977	0.11666	0.14254	0.632	0.1209	0.15117
5	0.33882	0.19212	0.28215	0.34012	0.16962	0.19147
Mean Performance Metrics:	0.5269 ± 0.2132	0.1285 ± 0.0519	0.1680 ± 0.0881	0.5211 ± 0.2563	0.1300 ± 0.0502	0.1569 ± 0.0494

	STEC (Kernel Function: linear, BoxConstraint (C): 0.1, Epsilon: 0.1)			WSTEC (Kernel Function: linear, BoxConstraint (C): 0.1, Epsilon: 0.1)		
Fold	**R^2**	**MAE**	**RMSE**	**R^2**	**MAE**	**RMSE**
1	0.86769	0.084654	0.089099	0.86927	0.074858	0.088566
2	0.85765	0.088565	0.092416	0.74146	0.093945	0.12671
3	0.78898	0.084129	0.086619	0.67879	0.10229	0.10887
4	0.88115	0.082863	0.084447	0.77668	0.10376	0.11776
5	0.77184	0.097528	0.11259	0.45933	0.14594	0.17331
Mean Performance Metrics:	0.83346 ± 0.049514	0.087548 ± 0.0059718	0.093033 ± 0.011325	0.7051 ± 0.1537	0.1042 ± 0.0260	0.1230 ± 0.0315

CONCLUSIONS

This paper presents the influence of texture bump height on the limiting values of nondimensional load capacity and nondimensional stiffness coefficients of a foil journal bearing. The limiting solutions are based on the compressible Reynolds equation for high bearing numbers. A texture bump region extent with critical values of extent along the circumferential direction on bearing surface provides higher load capacity. Increasing nondimensional texture bump height (H_b) leads to increase in the nondimensional load capacity (W), beyond a critical value of texture bump extent (θ_t). The location and extent of bump influence the nondimensional stiffness coefficients of a texture bump foil bearing at low eccentricity ratios. The nondimensional stiffness coefficients (K_{ij}) increase with increase in the non-dimensional texture bump height (H_b) at lower eccentricity ratios.

The texture bump region has potential to enhance the foil bearing characteristics at low eccentricity ratio operations.

The future research directions suggested based on the findings of this study include: (i) additional and different sets of input features, and (ii) development of enhanced machine learning models for deeper insights on prediction of influence of specific features on the performance metrics.

ACKNOWLEDGEMENT

The authors would like to acknowledge the support of SRM Institute of Science and Technology and MIT Art, Design and Technology University.

REFERENCES

Agustin, S. A., Shravankumar, C., & Rao, T. V. V. L. N. (2020). Limiting stiffness coefficients analysis of texture foil journal bearing. IOP Conf. Series: Materials Science and Engineering, 912, 022031.

Agustin, S.A., Shravankumar, C., Kumar, A.A.J., & Rao, T. V. V. L. N. (2024). Limiting Load Capacity and Stiffness Coefficients of Bump Recess Foil Journal Bearing with FGM. J. Vib. Eng. Technol. 12, 9089–9095.

Aydin, F., & Durgut, R. (2021). Estimation of wear performance of AZ91 alloy under dry sliding conditions using machine learning methods. Transactions of Nonferrous Metals Society of China, 31 (1), 125-137.

Baş, H., & Karabacak, Y. E. (2023). Machine learning-based prediction of friction torque and friction coefficient in statically loaded radial journal bearings. Tribology International, 186, 108592

Cartwright, S., Rothwell, B. C., Figueredo, G., Medina, H., Eastwick, C., Layton, J., & Ambrose, S. (2024). A machine learning-driven approach to predicting thermo-elasto-hydrodynamic lubrication in journal bearings. Tribology International, 196, 109670.

Hasan, M. S., Kordijazi, A., Rohatgi, P. K., & Nosonovsky, M. (2021). Triboinformatic modeling of dry friction and wear of aluminum base alloys using machine learning algorithms. Tribology International, 161, 107065

Hasan, M. S., Kordijazi, A., Rohatgi, P. K., & Nosonovsky, M. (2022b). Machine learning models of the transition from solid to liquid lubricated friction and wear in aluminum-graphite composites. Tribology International, 165, 107326

Hasan, M. S., Wong, T., Rohatgi, P. K., & Nosonovsky, M. (2022a). Analysis of the friction and wear of graphene reinforced aluminum metal matrix composites using machine learning models. Tribology International, 170, 107527.

Heshmat, H., Walowit, J. A., & Pinkus, O. (1983). Analysis of gas-lubricated foil journal bearings. Journal of Lubrication Technology, 105, 647–655.

Hulipalled, P., Algur, V., Lokesha, V., Saumya, S., & Satyanarayan. (2023). Interpretable ensemble machine learning framework to predict wear rate of modified ZA-27 alloy. Tribology International, 188, 108783.

Kim, T. H., & San Andrés L. (2007). Analysis of advanced gas foil bearings with piecewise linear elastic supports. Tribology International, 40(8), 1239–1245.

Lund, J. W. (1987). Review of the Concept of Dynamic Coefficients for Fluid Film Journal Bearings. ASME Journal of Lubrication Technology, 109(1), 37-41.

Marian, M., & Tremmel, S. (2021). Current Trends and Applications of Machine Learning in Tribology—A Review. Lubricants, 9(9), 86.

Marian, M., & Tremmel, S. (2023). Physics-Informed Machine Learning—An Emerging Trend in Tribology. Lubricants, 11(11), 463.

Marian, M., Mursak, J., Bartz, M. et al. (2023). Predicting EHL film thickness parameters by machine learning approaches. Friction, 11, 992–1013.

Mohammed A. J., Mohammed A. S., & Mohammed A. S. (2023). Prediction of Tribological Properties of UHMWPE/SiC Polymer Composites Using Machine Learning Techniques. Polymers. 15(20), 4057.

Mousavirad, S. J., et al. (2023). A transfer learning based artificial neural network in geometrical design of textured surfaces for tribological applications. Surf. Topogr.: Metrol. Prop. 11, 025001

Ning, H., Chen, F., Su, Y. et al. (2024). Modeling and prediction of tribological properties of copper/aluminum-graphite self-lubricating composites using machine learning algorithms. Friction, 12, 1322–1340.

Peng, J.-P., & Carpino, M. (1993). Calculation of Stiffness and Damping Coefficients for Elastically Supported Gas Foil Bearings. J. Tribol., 115(1), 20-27.

Peng, Z. C., & Khonsari, M. M. (2004a). On the limiting load carrying capacity of foil bearings. ASME Journal of Tribology, 126, 817-818

Peng, Z. C., & Khonsari, M. M. (2004b). Hydrodynamic analysis of compliant foil bearing with compressible air flow. ASME Journal of Tribology, 126, 542-546.
Radil, K., Howard, S., & Dykas, B. (2002). The Role of Radial Clearance on the Performance of Foil Air Bearings. Tribology Transactions, 45(4), 485–490.
Rahman, M. H., Shahriar, S., & Menezes, P. L. (2023). Recent Progress of Machine Learning Algorithms for the Oil and Lubricant Industry. Lubricants, 11(7), 289.
Rosenkranz, A., Marian, M., Profito, F. J., Aragon, N., & Shah R. (2021). The Use of Artificial Intelligence in Tribology—A Perspective. Lubricants, 9(1), 2.
Rubio, D., & San Andrés L. (2006). Bump-type foil bearing structural stiffness: experiments and predictions. Journal of Engineering for Gas Turbines and Power, 128, 653–660.
Samanta, P., Murmu, N. C., & Khonsari, M. M. (2019). The evolution of foil bearing technology. Tribology International, 135, 305–323.
Sawicki, J. T., & Rao, T. V. V. L. N. (2005). Limiting stiffness and damping coefficients of foil bearing. Proceedings of IDETC/CIE, 1069-1073.
Tremmel, S., & Marian, M. (2022). Machine Learning in Tribology, MDPI Books.
Yin, N., Xing, Z., He, K. et al. Tribo-informatics approaches in tribology research: A review. Friction 11, 2023, 1–22.
Yin, N., Yang, P., Liu, S. et al. (2024). AI for tribology: Present and future. Friction 12, 1060–1097.
Zhang, Z., & Yin, N. (2024). Tribo-Informatics: The Systematic Fusion of AI and Tribology (1st ed.). CRC Press.
Zhang, Z., Yin, N., Chen, S. et al. (2021). Tribo-informatics: Concept, architecture, and case study. Friction, 9, 642–655
Zhu, C., Jin, L., Li, W., Han, S., & Yan, J. (2024). The Prediction of Wear Depth Based on Machine Learning Algorithms. Lubricants, 12(2), 34.